Received: 15 September 2023 | Revised: 29 November 2023 | Accepted: 30 November 2023

DOI: 10.1002/alz.13659

Alzheimer's & Dementia®
THE JOURNAL OF THE ALZHEIMER'S ASSOCIATION

RESEARCH ARTICLE

Parenchymal CSF fraction is a measure of brain glymphatic clearance and positively associated with amyloid beta deposition on PET

Liangdong Zhou[1] | Thanh D. Nguyen[2] | Gloria C. Chiang[1,3] | Xiuyuan H. Wang[1] | Ke Xi[1] | Tsung-Wei Hu[1] | Emily B. Tanzi[1] | Tracy A. Butler[1] | Mony J. de Leon[1] | Yi Li[1]

[1]Department of Radiology, Brain Health Imaging Institute (BHII), Weill Cornell Medicine, New York, New York, USA

[2]Department of Radiology, MRI Research Institute (MRIRI), Weill Cornell Medicine, New York, New York, USA

[3]Department of Radiology, Division of Neuroradiology, Weill Cornell Medicine, New York-Presbyterian Hospital, New York, New York, USA

Correspondence
Yi Li, Department of Radiology, Brain Health Imaging Institute, Weill Cornell Medicine, 407 E 61st St., Feil-206, New York, NY 10065, USA.
Email: yil4008@med.cornell.edu

Funding information
National Institutes of Health; National Institute of Aging (NIA), Grant/Award Numbers: R01AG057848, R01AG068398, R01AG080011, RF1AG057570, R56AG058913, R21NS116516, R01AG057681, R56NS111052

Abstract

INTRODUCTION: Mapping of microscopic changes in the perivascular space (PVS) of the cerebral cortex, beyond magnetic resonance-visible PVS in white matter, may enhance our ability to diagnose Alzheimer's disease (AD) early.

METHODS: We used the cerebrospinal fluid (CSF) water fraction (CSFF), a magnetic resonance imaging–based biomarker, to characterize brain parenchymal CSF water, reflecting microscopic PVS in parenchyma. We measured CSFF and amyloid beta (Aβ) using ^{11}C Pittsburgh compound B positron emission tomography to investigate their relationship at both the subject and voxel levels.

RESULTS: Our research has demonstrated a positive correlation between the parenchymal CSFF, a non-invasive imaging biomarker indicative of parenchymal glymphatic clearance, and Aβ deposition, observed at both individual and voxel-based assessments in the posterior cingulate cortex.

DISCUSSION: This study shows that an increased parenchymal CSFF is associated with Aβ deposition, suggesting that CSFF could serve as a biomarker for brain glymphatic clearance, which can be used to detect early fluid changes in PVS predisposing individuals to the development of AD.

KEYWORDS
aging effect, Alzheimer's disease, amyloid beta, glymphatic clearance, magnetic resonance imaging, magnetic resonance transverse relaxation time relaxometry, parenchymal cerebrospinal fluid fraction, positron emission tomography

Highlights

- Cerebrospinal fluid fraction (CSFF) could be a biomarker of parenchymal perivascular space.
- CSFF is positively associated with amyloid beta (Aβ) deposition at subject level.

- CSFF in an Aβ+ region is higher than in an Aβ− region in the posterior cingulate cortex.
- Correspondence is found between Aβ deposition and glymphatic clearance deficits measured by CSFF.

1 | BACKGROUND

Glia-lymphatic (glymphatic) clearance deficits have recently gained attention as a major driver of the amyloid pathology seen in neurodegenerative conditions like Alzheimer's disease (AD).[1–3] Perivascular spaces (PVS) in the brain contain cerebrospinal fluid (CSF)–like fluid and constitute a key component of glymphatic clearance. Specifically, PVS enlargement is believed to reflect reduced CSF flow and impaired glymphatic clearance.[4] Although the pathophysiology of the enlargement of PVS is still not fully understood, it has been shown to be associated with a higher level of aquaporin-4, breakdown of the blood–brain barrier (BBB), cerebral amyloid angiopathy (CAA), hypertension, and small vessel disease (SVD).[5–9] We hypothesized an impaired drainage could be a potential cause of enlarged PVS due to fluid residue and stasis. The enlargement of PVS might further decrease the CSF flow due to more fluid away from the vessel wall and fluid accumulation.[10] The dysfunctional CSF clearance along with the enlargement of PVS can lead to the deposition and accumulation of extracellular amyloid beta (Aβ) plaques that can be quantified using positron emission tomography (PET) with various radiotracers.[1,11–13] Historically, PVS load has been associated with an array of conditions and has been quantified using T2-weighted magnetic resonance imaging (MRI) and image segmentation techniques. Limitations of PVS segmentation approaches include image quality and resolution, and also low detection of PVS at the sub-voxel level or within close proximity to arteries and veins.[14–16] We developed a three-compartment water model to characterize fluid within the brain, using multi-echo magnetic resonance transverse relaxation time (MR T2) relaxometry to quantify the parenchymal CSF fraction (CSFF), the intra-extracellular water fraction (IEWF), and the myelin water fraction (MWF).[17,18] According to biophysical principles, CSFF is the component of the total T2 signal with a long T2 time (T2 > 200 ms in 3T magnetic field) that theoretically corresponds to the freely mobile water that resides in the PVS.[19,20] Therefore, because PVS is a component of the glymphatic system, CSFF could serve as a biomarker of glymphatic clearance. Our previous study showed that the CSFF quadratically increases in the cerebral cortex (gray matter [GM]) and linearly increases with normal aging in deep gray matter (dGM) and cerebral white matter (WM), suggestive of decreased glymphatic function or more retention of glymphatic fluid in PVS and parenchyma with age.[21] Research on water homeostasis is not only important to healthy aging, but also to the understanding of the progression of neurodegenerative disease. For example, lower CSF clearance (vCSF) in the lateral ventricle (LV) and lower diffusivity of interstitial fluid along PVS (diffusion tensor image analysis along the perivascular space [DTI-ALPS]) has been shown to be associated with AD pathology.[12,22,23] Thus, changes in CSF in tissue (CSFF) could be sensitive enough to detect subtle developments in the pathology of PVS enlargement and serve as an early diagnostic biomarker.[21] This led us to further investigate the relationship between CSFF and established AD markers such as Aβ deposition, and to investigate whether AD status could be sufficiently inferred using CSFF data.[24]

In this study, we assessed the relationship between CSFF and brain Aβ deposition measured by ^{11}C-Pittsburgh compound B (PiB) PET in patients with mild cognitive impairment (MCI) or mild AD, and cognitively normal (CN) control subjects. We evaluated the effects of age and diagnostic group on CSFF. We specifically investigated the regional distribution of CSFF in the Aβ positive and negative voxels of the posterior cingulate cortex (PCC), a widely accepted region of early Aβ deposition in AD.[25–27] We hypothesized that increased CSFF would be associated with diagnostic group and regional Aβ deposition.

2 | METHODS

2.1 | Subjects

In this cross-sectional study, a total of 29 of subjects had both MR-based CSFF maps and PiB PET scans. Seven subjects were diagnosed with MCI that were Aβ− (PiB PET reading) and thus were excluded, as was one with multiple sclerosis (MS), leaving 21 eligible subjects. Seven of the 21 subjects were diagnosed as MCI/AD and 14 were CN. All studies were approved by the Weill Cornell Medicine Institutional Review Board and written informed consent was obtained from all participants.

2.2 | Subject assessment

All subjects underwent standardized evaluations by a cognitive neurologist. The evaluation consisted of a neurological exam, interviews with the subject and informant, Clinical Dementia Rating scale,[28] Montreal Cognitive Assessment,[29] the National Alzheimer's Coordinating Center (NACC) Uniform Data Set V3.0 telephone cognitive battery,[30] clinical blood tests, electrocardiogram, MRI, and amyloid (^{11}C-PiB) and tau (^{18}F-MK-6240) PET scanning. Subjects were assigned a final diagnosis by a board-certified neurologist (T.B.) in accordance with NACC criteria based on evaluation of all available information. The MRI and

PET examinations were reviewed by a board-certified radiologist with subspecialty certification in neuroradiology and 14 years of experience in diagnostic brain PET imaging (G.C.). All subjects were reviewed in a multidisciplinary consensus conference. Subjects included in this study were diagnosed as either CN or with MCI or mild dementia due to AD (MCI/AD).

2.3 | Image acquisition

2.3.1 | MRI images acquisition

All subjects underwent brain MRI studies on a Siemens Prisma 3T scanner (Siemens Healthineers) using a product 64-channel head/neck receiver coil. The brain imaging protocol consisted of 3D magnetization-prepared rapid acquisition gradient echo (MPRAGE) T1w and 3D T2-SPACE sequences for anatomical structural imaging, as well as 3D FAST-T2 sequence for mapping of water fractions (WF), and T2 fluid-attenuated inversion recovery (FLAIR) sequence for WM hyperintensity detection.[17] The imaging parameters were as follows:[21,31] (1) 3D sagittal T1 MPRAGE: repetition time (TR)/echo time (TE)/inversion time (TI) = 2300/2.3/900 ms, flip angle (FA) = 8°, readout bandwidth (rBW) = 200 Hz/pixel, voxel size = 1.0 mm isotropic, GRAPPA parallel imaging factor (R) = 2, scan time = 5.5 minutes; (2) 3D sagittal T2W SPACE: TR/TE = 3200/408 ms, FA = 90°, rBW = 751 Hz/pixel, turbo factor = 285, voxel size = 1.0 mm isotropic; (3) 3D axial FAST-T2 at two slice thickness: spiral TR/TE = 7.8/0.5 ms, nominal T2prep times = 0 (T2-prep turned off), 7.5, 17.5, 67.5, 147.5, and 307.5 ms, FA = 10°, rBW = 1042 Hz/pixel, number of spiral leaves per stack = 32, number of spiral leaves collected per T2prep = 64, voxel size = $1.3 \times 1.3 \times 2$ mm^3 (scan time = 7 minutes); (4) 3D sagittal FLAIR SPACE with fat saturation: TR/TE/TI = 4000/384/2400 ms, echo spacing = 3.46 ms, FA = 90°, rBW = 751 Hz/pixel, turbo factor = 278, voxel size = 1.0 mm isotropic, R = 2, scan time = 5.4 minutes.

2.3.2 | PET images acquisition

PiB PET image was acquired using a Siemens Biograph mCT–S (64) slice PET/CT. PiB was synthesized by the institutional radiochemistry facility. The data was acquired in list mode from 40 to 90 minutes after a rapid bolus injection of ≈555 MBq. PiB PET images were reconstructed to a $512 \times 512 \times 74$ matrix of $0.8 \times 0.8 \times 3$ mm voxels in 5×10 minute time frames from 40 to 90 minutes with list mode.

2.4 | Image processing

2.4.1 | MRI region of interest parcellation

T1w MRI was regionally segmented using FreeSurfer (FS)[32] version 7.1 recon-all command for region of interest (ROI) parcellation with the assistance of T2w to enhance segmentation quality. ROIs consisted of the bilateral cerebellar cortex as a reference region for Aβ standardized uptake value ratio (SUVR) determination, and an ROI encompassing the bilateral parietal, frontal, and temporal ROI, were collectively referred to as the AD cortical mask (ADmask) for quantifying Aβ.[25] ROIs for CSFF values included: ADmask and posterior cingulate cortex (PCC) were extracted from FS aparc+aseg segmentation file matched with FS look-up-table (LUT). To reduce partial volume effect (PVE), all ROIs for CSFF calculation were eroded according to the image resolution. Specifically, for CSFF, the ROI anisotropic erosion was done with Gaussian kernel sized $1.3 \times 1.3 \times 2$ mm^3. All ROIs for PET SUVR calculation were eroded by one voxel using 3D sphere kernel to minimize the PVE.

2.4.2 | PET SUVR

Summed PiB PET data from 60 to 90 minutes were used for SUVR calculation. Specifically, all the dynamic frames were realigned to the summed images between 40 and 90 minutes, and the summed image was then coregistered to the T1w in FS space using the normalized mutual information method in FSL.[33] SUVR was calculated using the cerebellar cortex as a reference region.[34] Average SUVR within the cortical ADmask served as the overall measure of Aβ deposition.[25]

RESEARCH IN CONTEXT

1. **Systematic review**: The authors reviewed existing literature on the application of cerebrospinal fluid fraction (CSFF) mapping, a subvoxel-level measure of fluid in perivascular space (PVS), on Alzheimer's disease (AD) (PubMed, Google Scholar). Published studies in similar areas were the application of diffusion tensor imaging-based free water (DTI-FW) mapping, which is mapping the total extracellular water including water in both PVS and interstitial space.
2. **Interpretation**: This study shows that parenchymal CSFF is positively associated with the amyloid beta (Aβ) deposition measured by ^{11}C-Pittsburgh compound B positron emission tomography at the subject level. At the voxel level, the results show that an elevated CSFF is associated with the Aβ+ voxels in posterior cingulate cortex compared to Aβ− voxels, indicating that Aβ deposition is caused by glymphatic clearance deficits.
3. **Future directions**: Further validation of the relationship between CSFF and PVS pathology will be helpful to confirm and push the use of CSFF mapping to the next level.

At the voxel level, PCC Aβ+ and Aβ− voxels were defined by using SUVR cut-off 1.65, and combined to form ROIs denoted as Aβ+ and Aβ− ROIs, respectively.[25,35] Aβ+ and Aβ− ROIs were then intersected with PCC, respectively, to get finalized Aβ+ and Aβ− ROIs for CSFF values calculation.

2.4.3 | CSFF mapping

CSFF, IEWF, and MWF maps were obtained using non-linear least square fitting of the 3-exponential model with L2 regularization. The input data of the fitting process was the 6 echo FAST-T2 data with degibbs and denoising processing. CSFF is the component corresponding to a long T2 (T2 > 200 ms) signal and was constrained in the fitting process. The details of the mapping procedure were documented in our previous publications.[17,21] The CSFF mapping in this study was done identically with the same in-house processing pipeline. The water maps were rigidly coregistered to FS T1w space using normalized mutual information criteria. The ROI values of CSFF were extracted by averaging the CSFF in all the voxels of the ROI.

2.5 | Statistical analysis

Statistical analyses were performed in RStudio Version 2022.7 (RStudio PBC) and MATLAB Version 2023a (MathWorks). First, we tested sex differences in the continuous variables like CSFF, PiB SUVR, and age using the Wilcoxon rank sum test, and of binary variables like the diagnostic group and Aβ status using Pearson chi-square test. Second, we performed the subject-level analysis of the relationship between CSFF and PiB SUVR in ADmask using linear regression by controlling for age and sex. Third, we evaluated the association between CSFF and age in both CN and MCI/AD groups using multivariable regression analysis controlling for sex. An independent two-sample *t* test was used to test the difference of CSFF between CN and MCI/AD subjects. Fourth, we performed the tests of regional CSFF distribution in Aβ+ and Aβ− subregions of PCC using the paired Wilcoxon rank sum test. Finally, we conducted the effects of Aβ positivity threshold of PiB SUVR on regional CSFF in PCC by incrementally changing the threshold from 1.45 to 1.9 with a step size of 0.05, and the paired *t* test was used to compare the CSFF in Aβ+ and Aβ− subregions. The significance level of all tests and analyses was set to $P < 0.05$. Note that all *r* reported is the correlation coefficient and R^2 is adjusted *R*-squared values.

2.6 | Data availability

Raw data were generated at the Brain Health Imaging Institute (BHII) at Weill Cornell Medicine. Derived data supporting the findings of this study are available from the corresponding author on reasonable request.

3 | RESULTS

3.1 | Subject information

The subjects' demographic and clinical information is listed in Table 1. The last column in Table 1 is the *P* value for each measure compared by diagnostic group. Among the 21 subjects, there were 10 Aβ+ and 11 Aβ− subjects. Among those 10 Aβ+ subjects, 7 were MCI/AD and 3 were CN.

Age, diagnostic group, ADmask PiB SUVR, PCC PiB SUVR, ADmask CSFF, and PCC CSFF did not significantly differ between sexes, that is, $P > 0.05$ for all the tests.

3.2 | Water maps

Water maps were reconstructed using the 6 TE FAST-T2 data. Figure 1 shows the three water maps of a 72-year-old male with MCI/AD. From left to right are (A) CSFF, (B) IEWF, and (C) MWF, respectively. CSFF is defined as CSFF = 100 − (IEWF + MWF) in percent.

3.3 | CSFF for Aβ deposition

Linear regression between PiB SUVR in ADmask and CSFF controlling for age and sex was performed. Figure 2 presents the partial regression plots between Aβ deposition measured by PiB SUVR in ADmask and CSFF (Figure 2A) and age (Figure 2B). We show in Figure 2A that PiB SUVR is positively associated with CSFF in the linear regression ($t = 5.355$, $P < 0.0001$, $R^2 = 0.609$) and has no association with age ($P = 0.377$) in Figure 2B. According to the plots, a combination of CSFF and PiB SUVR can distinguish most MCI/AD subjects from CN.

3.4 | CSFF for aging and diagnosis

To investigate the effect of age on CSFF, we performed a linear regression between CSFF and age, sex, and diagnosis. Figure 3 displays the significant relationship between CSFF and age by the diagnostic group showing Pearson correlation coefficients by group (all subjects: $r = 0.534$, $P < 0.05$; CN: $r = 0.646$, $P < 0.05$; MCI/AD: $r = 0.498$, $P = 0.255$). These data show that CSFF, as a potential biomarker for deficits of glymphatic clearance, increases with age and MCI/AD. Figure 3A is the regression plots between CSFF and age (age: $t = 2.873$, $P < 0.01$, Dx MCI/AD: $t = 4.496$, $P < 0.001$, $R^2 = 0.618$) controlling for sex. Restricting the analysis for only CN subjects, the regression model still shows a significant relationship between increased CSFF with age ($t = 3.243$, $P < 0.05$, $R^2 = 0.398$), which is consistent with previous results.[21] However, restricting the analysis to only MCI subjects, the CSFF was not significantly associated with age ($t = 1.428$, $P = 0.227$, $R^2 = 0.009$). In Figure 3B the boxplot shows a significant difference of CSFF between CN and MCI/AD ($P < 0.01$).

TABLE 1 Subjects' demographics and clinical information. The last column is the *P* value for diagnostic group differences on each measure.

Item	Overall	CN	MCI/AD	*P* value
Subjects number	21	14	7	–
Sex = M (%)	6 (28.6)	4 (28.6)	2 (28.6)	1
Age (mean [SD])	66.62 (12.58)	64.79 (13.62)	70.29 (11.18)	0.411
Aβ reading status = positive (%)	10 (47.6)	3 (21.4)	7 (100)	<0.01
ADmask PiB SUVR (mean [SD])	1.58 (0.67)	1.18 (0.16)	2.39 (0.57)	<0.001
PCC PiB SUVR (mean [SD])	1.72 (0.74)	1.3 (0.22)	2.56 (0.69)	<0.001
ADmask CSFF (mean [SD])	5.13 (0.57)	4.85 (0.34)	5.70 (0.51)	<0.001
PCC CSFF (mean [SD])	7.13 (1.01)	6.86 (0.76)	7.65 (1.29)	<0.01

Abbreviations: Aβ, amyloid beta; AD, Alzheimer's disease; ADmask, Alzheimer's disease cortical mask; CN, cognitively normal; CSFF, cerebrospinal fluid water fraction; MCI, mild cognitive impairment; PCC, posterior cingulate cortex; PiB, Pittsburgh compound B; SD, standard deviation; SUVR, standardized uptake value ratio.

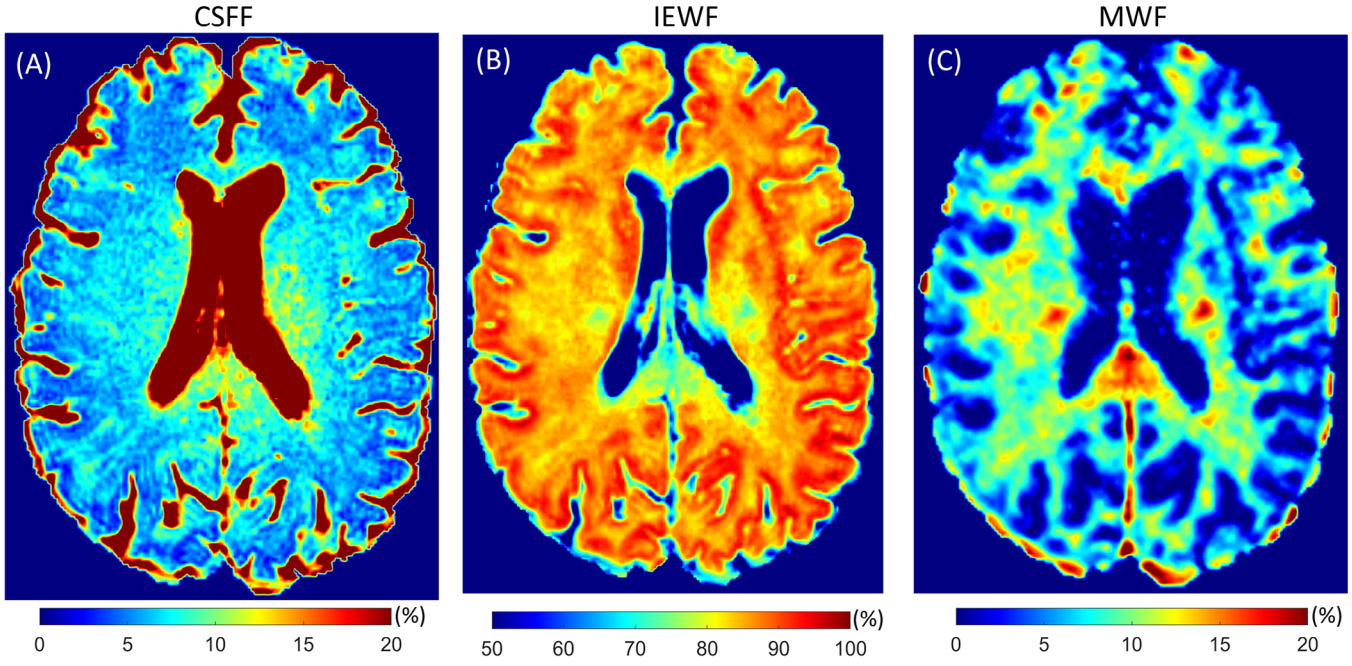

FIGURE 1 CSF fraction, intra-extracellular water fraction, and myelin water fraction water maps derived from three-water model using multi-echo MR FAST-T2 data. The maps are from a 72-year-old male subject with MCI/AD: (A) CSFF for long T2 component (T2: 200–2000 ms) of multi-echo T2 signal; (B) IEWF for intermediate T2 component (T2: 20–200 ms); and (C) MWF for short T2 component (T2: 5–20 ms). AD, Alzheimer's disease; CSF, cerebrospinal fluid; CSFF, cerebrospinal fluid water fraction; IEWF, intra-extracellular water fraction; MCI, mild cognitive impairment; MR, magnetic resonance; MWF, myelin water fraction.

3.5 | Regional CSFF in Aβ positive and negative regions

We performed tests of regional CSFF distribution in Aβ+ and Aβ− regions of the PCC. Figure 4 shows the Aβ+ and Aβ− subregions in the PCC for a 63-year-old female CN subject. Figure 4A-4C shows the Aβ+ and Aβ− masks overlaid on the T1w image in sagittal, coronal, and axial views, and Figure 4D-F shows the same masks on the PiB SUVR image. Figure 5 presents the results of increased CSFF values in Aβ+ compared to Aβ+ ROIs of PCC by diagnostic group. Figure 5A,C are the Bland–Altman plots of the comparison between CSFF in Aβ+ and Aβ− subregions, for CN and MCI/AD groups, respectively. It clearly shows that all the points are located within the 95% confidence interval with positive bias, meaning that CSFF in an Aβ+ region is higher than that in an Aβ− region. Figure 5B shows the CSFF changes between Aβ+ and Aβ− regions among 14 CN subjects, Wilcoxon rank sum test shows that the Aβ+ region has a higher CSFF than that in the Aβ− region ($P < 0.01$). Figure 5D shows the CSFF change between Aβ+ and Aβ− regions among seven MCI/AD subjects. There are four MCI/AD subjects with no Aβ− region in the PCC because the PiB SUVR in PCC is

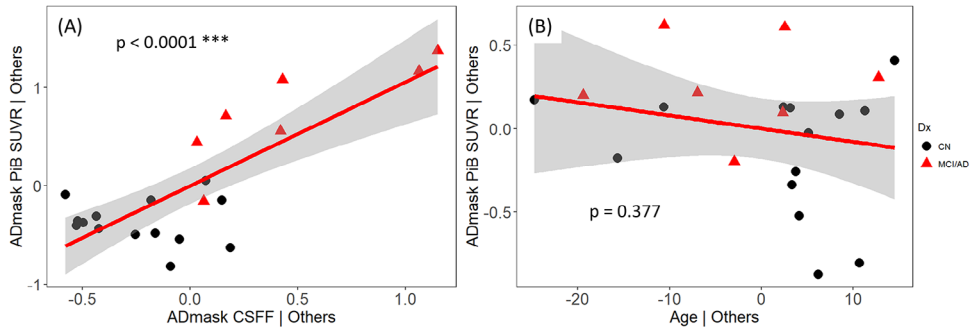

FIGURE 2 The partial regression plots from multivariable analyses between beta-amyloid deposition measured by PiB PET SUVR in ADmask, CSFF, and age: (A) partial regression plots between PiB PET SUVR and CSFF in ADmask; (B) partial regression plots between PiB PET SUVR and age. Black dots represent CN subjects and red triangles indicate MCI/AD subjects. We see that PiB SUVR positively associates with CSFF, and there is no association with age. AD, Alzheimer's disease; ADmask, Alzheimer's disease cortical mask; CN, cognitively normal; CSFF, cerebrospinal fluid water fraction; MCI, mild cognitive impairment; PET, positron emission tomography; PiB, Pittsburgh compound B; SUVR, standardized uptake value ratio.

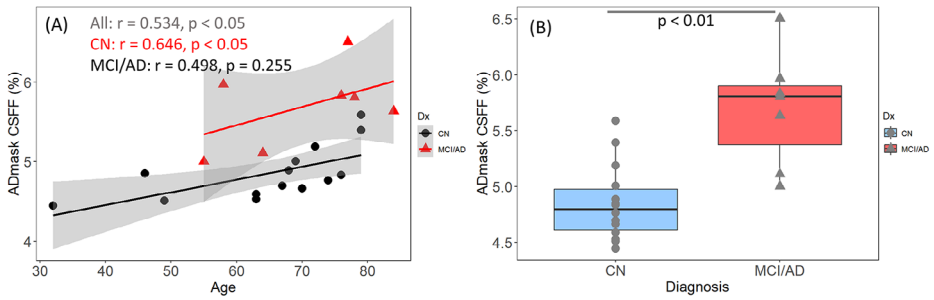

FIGURE 3 The relationship between ADmask CSFF and age by diagnostic group: (A) the regression plot between CSFF and age by group; (B) boxplot of CSFF by diagnosis. (A) Shows that CSFF increases with age in both MCI/AD and CN subjects with positive correlation coefficients. There is an elevation of CSFF for MCI/AD compared to CN controlled for age ($P < 0.01$). (B) Shows significant increase in CSFF in MCI/AD compared to CN subjects. AD, Alzheimer's disease; ADmask, Alzheimer's disease cortical mask; CN, cognitively normal; CSFF, cerebrospinal fluid water fraction; MCI, mild cognitive impairment; PET, positron emission tomography; PiB, Pittsburgh compound B; SUVR, standardized uptake value ratio.

> 1.65 in all voxels. Consequently, there is no available CSFF in these Aβ− regions.

In the evaluation of the association between PiB SUVR and CSFF in PCC, a linear regression controlling for age and sex was performed and it was discovered that the PiB SUVR is significantly associated with CSFF ($n = 21$, $P < 0.05$, $R^2 = 0.239$).

3.6 | Effects of Aβ positivity threshold on regional CSFF

The effect of Aβ+ threshold of PiB PET SUVR on CSFF in PCC was evaluated with results presented in Figure 6. It shows the CSFF differences between Aβ+ and Aβ− regions in PCC with variable thresholds from 1.55 to 1.9 in the CN group. The CSFF differences on all thresholds are significantly greater than zero. We also observe an increasing CSFF in Aβ+ region as the PiB SUVR threshold increases. These results imply that the observed CSFF gap between Aβ+ and Aβ− regions is not sensitive to the threshold on PiB SUVR and warrants CSFF as a consistent biomarker across Aβ levels.

4 | DISCUSSION

Our study presents a significant association between the MR T2 relaxometry-based CSFF and Aβdeposition assessed by PiB PET, suggesting CSFF as a potential biomarker for glymphatic clearance in AD. Key findings include: (1) an increase in Aβ deposition with CSFF at the subject level, (2) differentiation of CN from MCI/AD based on CSFF, and (3) higher voxel-level CSFF in Aβ+ regions compared to Aβ− regions in CN subjects.

4.1 | PVS as a glymphatic clearance pathway

PVS are cavities filled with CSF-like fluid surrounding the blood vessels in the brain.[36,37] They are instrumental in the brain's waste clearance system, including the removal of Aβ.[2,4,38] Varied research outcomes have linked PVS load to Aβ deposition, yet inconsistencies may arise from measurement sensitivity.[14,16,39] PVS enlargement may reflect CSF fluid stasis and reduced flow leading to overall deficits in glymphatic clearance[40–42] because PVS load segmentation depends on

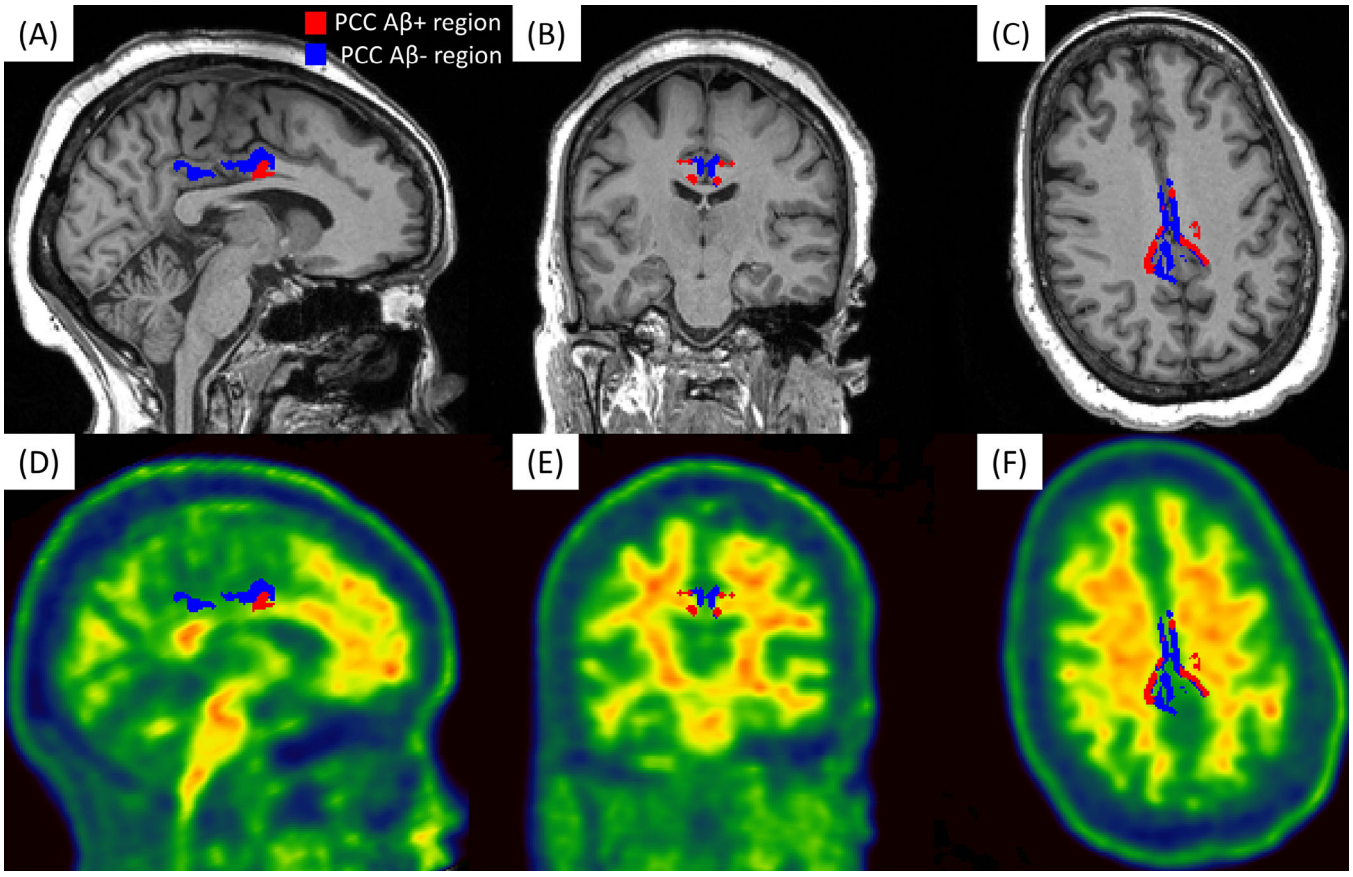

FIGURE 4 Example of Aβ+ and Aβ- regions in PCC; (A–C) are Aβ+ and Aβ− masks on T1w sagittal, coronal, and axial views, respectively; and (D–F) overlays of the masks on PiB PET SUVR map. The red region is for Aβ+ voxels and the blue region is for Aβ− voxels. Please note that the masks were dilated 1 voxel from the outside to enhance the visibility. Aβ, amyloid beta; PCC, posterior cingulate cortex; PET, positron emission tomography; PiB, Pittsburgh compound B; SUVR, standardized uptake value ratio.

image (typically T2w) resolution and quality,[15,43,44] and only includes the visibly enlarged PVS surrounding periarteries in WM.[45,46] Our CSFF potentially overcomes these limitations by accounting for all parenchymal CSF water in PVS, including microscale PVS that traditional imaging might miss.

4.2 | CSFF as glymphatic clearance biomarker for global Aβ deposition

Glymphatic clearance deficits are hypothesized to be associated with Aβ deposition due to impaired clearance of Aβ.[31,38] Our results indicate a positive association between Aβ deposition and CSFF, underscoring its potential as a predictor of Aβ deposition. This is especially pertinent as increased CSFF may reflect PVS enlargement, suggesting impaired glymphatic clearance. We aim to further explore CSFF's predictive capacity through model training on larger datasets.

CSFF is a measure of the portion of the voxel that can be attributed to CSF by modeling the MR T2 signal into three water components.[21] This approach of mapping water fractions was first proposed to map myelin water (MWF, short T2 [5–20 ms] component) in the brain for multiple sclerosis studies.[17,18,47] In contrast, CSFF accounts for the long T2 (200–2000 ms) component and theoretically corresponds to the signal of freely mobile water, that is, the CSF (or CSF-like) water. The third component in the model accounts for the IEWF corresponding to the signal of intermediate range of T2 (20–200 ms). The underlying mechanism is that the T2 relaxation time of water is affected by the microenvironment of the molecules: myelin water is confined in the myelin sheath, intra-extracellular water is constrained in intracellular space or bounded within the extracellular matrix, and the CSF water in PVS is freely movable in a relatively large space, as illustrated in Figure 7.[48–50] The advantage of CSFF is that it maps parenchymal CSF water in both periarterial and perivenous spaces at macroscale and microscale. To the best of our knowledge, CSFF is the first biomarker that is able to detect subvoxel brain CSF water in AD rendering CSFF a promising biomarker for early, subtle change of PVS pathology and glymphatic clearance deficits. It is worth noting that CSFF mapping should be distinguished from the free water mapping in diffusion tensor imaging (DTI-FW).[51] DTI-FW is a mapping of a combination of interstitial fluid (ISF) and CSF in PVS assuming their isotropic diffusivity.[52,53] DTI-FW for the normal brain has a greater number than CSFF (DTI-FW in GM: 30%–60% vs. CSFF in GM: 4%–9%).[21,53] PVS load has been supposed to be at a similar scale as the cerebral blood volume (CBV: 3%–5%) in the human brain,[9] which might

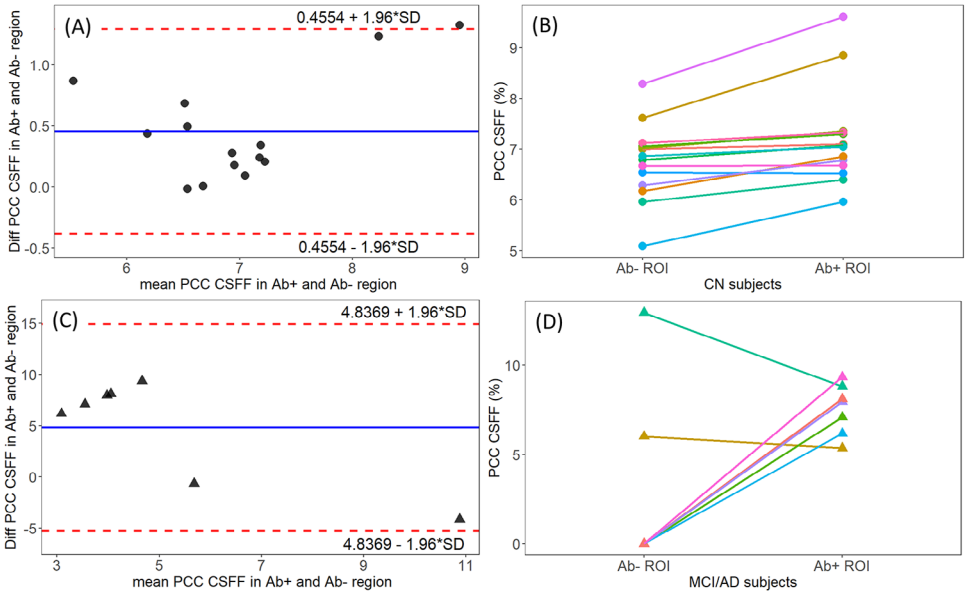

FIGURE 5 The results of CSFF values in Aβ+ and Aβ− subregions of PCC by diagnostic group. (A) and (B) are plots and comparisons of CSFF in PCC Aβ+ and Aβ− subregions for CN subjects. (C) and (D) are plots of CSFF change between in PCC Aβ+ and Aβ− subregions for MCI/AD subjects. In (A) and (C), each point represents a subject. In (B) and (D), each pair of connected points represents the change of CSFF for one subject. We see in CN group, CSFF in Aβ+ regions are significantly higher than that for Aβ− regions. Aβ, amyloid beta; AD, Alzheimer's disease; CN, cognitively normal; CSFF, cerebrospinal fluid water fraction; MCI, mild cognitive impairment; PCC, posterior cingulate cortex; PET, positron emission tomography; PiB, Pittsburgh compound B; SUVR, standardized uptake value ratio.

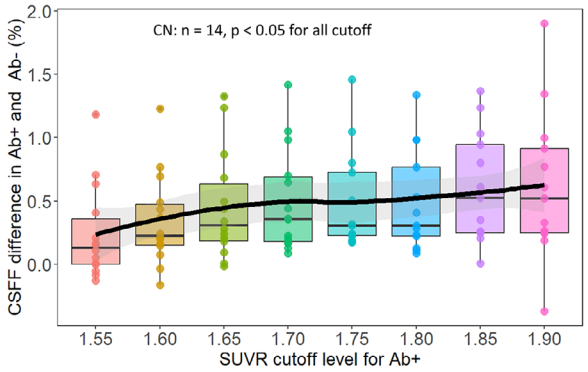

FIGURE 6 The effect of Aβ+ threshold of PiB PET SUVR on CSFF in PCC. In the CN group, CSFF is different between Aβ+ and Aβ− regions in PCC with variable thresholds from 1.55 to 1.9. The CSFF differences on all thresholds are significantly greater than zero. We also observe an increasing CSFF in the Aβ+ region as the PiB SUVR threshold increases. Aβ, amyloid beta; AD, Alzheimer's disease; CN, cognitively normal; CSFF, cerebrospinal fluid water fraction; MCI, mild cognitive impairment; PCC, posterior cingulate cortex; PET, positron emission tomography; PiB, Pittsburgh compound B; SUVR, standardized uptake value ratio.

be inferred from mice research where it has been shown a ratio of 1.12 to 1.88 between PVS to vessel cross-sectional area.[54] Therefore, CSFF is a more PVS volume-centered measure, while the DTI-FW is an extracellular space–dominated measure.

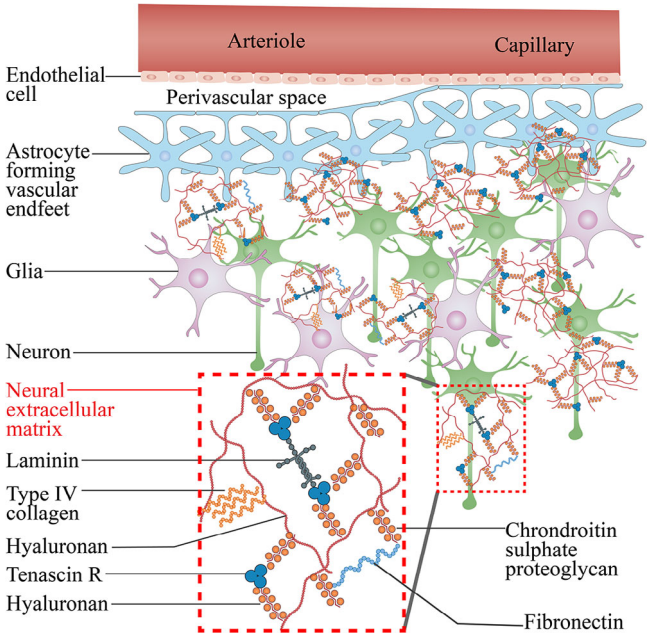

FIGURE 7 An illustration of perivascular space (PVS), intracellular space, and extracellular space shows the different microenvironments of water components. The fluid in PVS is CSF-like water, which is freely movable with long MR T2 time. The water in extracellular space is constrained by the extracellular matrix, which decreases the MR T2 time of the water molecule (modified from Figure 1 in Lau et al.[49]). CSF, cerebrospinal fluid; MR, magnetic resonance.

4.3 | CSFF for aging and diagnosis

CSF clearance in LV decreases with aging and is linked to AD imaging markers.[12,22] Glymphatic clearance relies on two interconnected fluid systems: the traditional CSF system and the newly characterized glymphatic pathways. The interplay between bulk CSF flow and glymphatic clearance has been a topic of growing interest. The microscale CSF flow in PVS could reveal subtle changes in pathology although the LV CSF clearance bulk flow plays a significant role in AD.[1,23] Our data replicates previous findings, showing an age-related increase in parenchymal CSFF among CN subjects.[21] These results could implicate an association between lower CSF turnover in LV and higher CSFF in the brain parenchyma in normal aging. Although we did not find a significant aging effect in MCI/AD subjects due to sample size and variation, elevated CSFF in MCI/AD compared to CN subjects may hint at reduced CSF turnover. This aligns with other findings but provides a novel focus on AD-related changes in the cerebral cortex. It is widely recognized that PVS segmentation in GM is impossible with standard 3T MRI giving limited image resolution. PVS pathology in WM is highly variable due to many factors including SVD, age, inflammation, and other diseases.[55] The variation in PVS among subjects reduces the specificity of using segmented PVS as a biomarker for early MCI/AD detection.

4.4 | CSFF correspondence with regional Aβ deposition

Given the advantages of CSFF mapping in GM for the subvoxel CSF in PVS, our regional observation of CSFF and Aβ deposition improves our mechanistic understanding of AD lesion formation. Previous studies have shown that the PCC is probably the earliest region of Aβ accumulation.[25–27] Our data are concordant with that principle given the higher PiB SUVR in PCC than GM. Evaluating Aβ deposition in an early-stage region like the PCC, we observed higher CSFF in Aβ+ subregions within CN individuals. While not significant in MCI/AD subjects, this could be attributed to the small sample size and the prevalence of Aβ+ voxels in PCC. The data suggest that CSFF is sensitive to early Aβ deposition. The ability of CSFF demonstrates subvoxel-level accuracy of CSF water mapping for microscopic PVS, namely in GM where conventional PVS segmentation methods may face challenges. It should be noted that because CAA shows significant Aβ deposition in amyloid PET and is associated with PVS enlargement clinical conditions such as CAA may affect the relationship between CSFF and brain amyloid measure. In this study, we have carefully excluded patients with severe CAA.

4.5 | Other glymphatic function measurements

There are other developed non-invasive measures for estimating glymphatic function in humans other than the CSFF reported in this work, including the PVS load by segmentation and DTI-ALPS. PVS segmentation can be performed on T2w but is only feasible for significantly enlarged ones in WM and the segmentation results vary across techniques and image quality.[15,43] DTI-ALPS is a method that computes fluid diffusivity along PVS, which potentially reflects the glymphatic function.[23,31,56,57] However, DTI-ALPS is only a representative global measure and inherently lacks information in local regions. A recent study has shown that DTI-ALPS might be associated with later stage Aβ deposition.[23] Compared to PVS load and DTI-ALPS, our proposed parenchymal CSFF offers an approach of whole brain mapping of subvoxel CSF distribution and potential early detection of glymphatic clearance deficits and Aβ deposition. While existing imaging tools in human study offer insights into glymphatic function, they each provide limited perspectives and there is an absence of universally recognized measurement techniques. A multimodal imaging approach could provide a more comprehensive understanding of fluid dynamics and clearance processes in the brain and might serve as a future research direction.[23]

4.6 | Limitations of this study

Although the results are promising, the study is not without limitations. First, the study is limited by a small sample size. It is difficult for elderly subjects to remain still during a 90 minute scanning protocol, especially for MCI/AD subjects. These results are expected to be confirmed and validated in a larger cohort as part of our ongoing research with an optimized protocol. Second, cross-sectional studies do not reveal a longitudinal or causal relationship between CSFF and Aβ deposition. We are currently collecting follow-up data on those subjects to further validate the early detection of Aβ deposition using CSFF. Third, validation of the association between CSFF and total PVS is not yet established. PVS load segmentation from MR images is limited by resolution that may only include a percentage of the total brain PVS. The validation between these two measures could be performed in histology studies with corresponding MRI scanning in animal models or in phantom experiments.

5 | CONCLUSIONS

Our research has demonstrated a correlation between the parenchymal CSFF, a non-invasive imaging biomarker indicative of parenchymal glymphatic clearance, and Aβ deposition, observed at both individual and voxel-based assessments in amyloid-vulnerable regions. These findings contribute to a more sophisticated comprehension of the localized deficits in glymphatic clearance associated with AD.

ACKNOWLEDGMENTS

This research was supported in part by the National Institutes of Health (NIH) National Institute of Aging (NIA) grants R01AG057848, R01AG068398, R01AG080011, RF1 AG057570, R56 AG058913, R21NS116516, R01AG057681, and R56NS111052. We thank the WCM radiochemistry team headed by Dr. James Kelly with the CBIC

team (Drs. Stefan Guhlke, Keunpoong Lim, Nicole Waterhouse, Ruth Fernandez, Islami Besim, and Eva Burnazi) and Drs. Simon Morim, Jonathan P. Dyke, and Edward K. Fung for PET data collection, and Dr. Silky Pahlajani for clinical assessments. We also sincerely thank the anonymous reviewers for their insightful and thoughtful comments that greatly improved this manuscript.

CONFLICT OF INTEREST STATEMENT

The authors have no relevant financial or non-financial interests to disclose. All the authors declare no competing interest in the present study. Author disclosures are available in the supporting Information.

CONSENT STATEMENT

All studies were approved by the Weill Cornell Medicine Institutional Review Board and written informed consent was obtained from all participants.

REFERENCES

1. Tarasoff-Conway JM, Carare RO, Osorio RS, et al. Clearance systems in the brain—implications for Alzheimer disease. *Nat Rev Neurol*. 2015;11(8):457-470. doi:10.1038/nrneurol.2015.119
2. Benveniste H, Liu X, Koundal S, Sanggaard S, Lee H, Wardlaw J. The glymphatic system and waste clearance with brain aging: a review. *Gerontology*. 2019;65(2):106-119. doi:10.1159/000490349
3. Iliff JJ, Wang M, Liao Y, et al. A paravascular pathway facilitates CSF flow through the brain parenchyma and the clearance of interstitial solutes, including amyloid β. *Sci Transl Med*. 2012;4(147):147ra111-147ra111. doi:10.1126/scitranslmed.3003748
4. Gouveia-Freitas K, Bastos-Leite AJ. Perivascular spaces and brain waste clearance systems: relevance for neurodegenerative and cerebrovascular pathology. *Neuroradiology*. 2021;63(10):1581-1597. doi:10.1007/s00234-021-02718-7
5. Sacchi L, Arcaro M, Carandini T, et al. Association between enlarged perivascular spaces and cerebrospinal fluid aquaporin-4 and tau levels: report from a memory clinic. *Front Aging Neurosci*. 2023;15(1191714):1-6. doi:10.3389/fnagi.2023.1191714
6. van Veluw SJ, Biessels GJ, Bouvy WH, et al. Cerebral amyloid angiopathy severity is linked to dilation of juxtacortical perivascular spaces. *J Cereb Blood Flow Metab*. 2016;36(3):576-580. doi:10.1177/0271678x15620434
7. Kamagata K, Andica C, Takabayashi K, et al. Association of MRI indices of glymphatic system with amyloid deposition and cognition in mild cognitive impairment and Alzheimer disease. *Neurology*. 2022;99(24):e2648-e2660. doi:10.1212/WNL.0000000000201300
8. Voorter PHM, van Dinther M, Jansen WJ, et al. Blood–brain barrier disruption and perivascular spaces in small vessel disease and neurodegenerative diseases: a review on MRI methods and insights. *J Magn Reson Imaging*. 2023:1-15. doi:10.1002/jmri.28989
9. Mestre H, Tithof J, Du T, et al. Flow of cerebrospinal fluid is driven by arterial pulsations and is reduced in hypertension. *Nat Commun*. 2018;9(1):4878. doi:10.1038/s41467-018-07318-3
10. Thomas JH. Fluid dynamics of cerebrospinal fluid flow in perivascular spaces. *J R Soc Interface*. 2019;16(159):20190572. doi:10.1098/rsif.2019.0572
11. Harrison IF, Ismail O, Machhada A, et al. Impaired glymphatic function and clearance of tau in an Alzheimer's disease model. *Brain*. 2020;143(8):2576-2593. doi:10.1093/brain/awaa179
12. Li Y, Rusinek H, Butler T, et al. Decreased CSF clearance and increased brain amyloid in Alzheimer's disease. *Fluids Barriers CNS*. 2022;19(1):21. doi:10.1186/s12987-022-00318-y
13. Mawuenyega KG, Sigurdson W, Ovod V, et al. Decreased clearance of CNS β-Amyloid in Alzheimer's disease. *Science*. 2010;330(6012):1774-1774. doi:10.1126/science.1197623
14. Kim HJ, Cho H, Park M, et al. MRI-visible perivascular spaces in the centrum semiovale are associated with brain amyloid deposition in patients with Alzheimer disease–related cognitive impairment. *Am J Neuroradiol*. 2021;42(7):1231-1238. doi:10.3174/ajnr.A7155
15. Sepehrband F, Barisano G, Sheikh-Bahaei N, et al. Image processing approaches to enhance perivascular space visibility and quantification using MRI. *Sci Rep*. 2019;9(1):12351. doi:10.1038/s41598-019-48910-x
16. Banerjee G, Kim HJ, Fox Z, et al. MRI-visible perivascular space location is associated with Alzheimer's disease independently of amyloid burden. *Brain*. 2017;140(4):1107-1116. doi:10.1093/brain/awx003
17. Nguyen TD, Deh K, Monohan E, et al. Feasibility and reproducibility of whole brain myelin water mapping in 4 minutes using fast acquisition with spiral trajectory and adiabatic T2prep (FAST-T2) at 3T. *Magn Reson Med*. 2016;76(2):456-465. doi:10.1002/mrm.25877
18. Nguyen TD, Wisnieff C, Cooper MA, et al. T2prep three-dimensional spiral imaging with efficient whole brain coverage for myelin water quantification at 1.5 tesla. *Magn Reson Med*. 2012;67(3):614-621. doi:10.1002/mrm.24128
19. Bontempi P, Rozzanigo U, Amelio D, Scartoni D, Amichetti M, Farace P. Quantitative multicomponent T2 relaxation showed greater sensitivity than flair imaging to detect subtle alterations at the periphery of lower grade gliomas. *Front Oncol*. 2021;11(651137):1-9. doi:10.3389/fonc.2021.651137
20. Daoust A, Dodd S, Nair G, et al. Transverse relaxation of cerebrospinal fluid depends on glucose concentration. *Magn Reson Imaging*. 2017;44:72-81. doi:10.1016/j.mri.2017.08.001
21. Zhou L, Li Y, Sweeney EM, et al. Association of brain tissue cerebrospinal fluid fraction with age in healthy cognitively normal adults. *Front Aging Neurosci*. 2023;15(1162001):1-6. doi:10.3389/fnagi.2023.1162001
22. de Leon MJ, Li Y, Okamura N, et al. Cerebrospinal fluid clearance in Alzheimer disease measured with dynamic PET. *J Nucl Med*. 2017;58(9):1471-1476. doi:10.2967/jnumed.116.187211
23. Zhou L, Butler TA, Wang XH, et al. Multimodal assessment of brain fluid clearance is associated with amyloid-beta deposition in humans. *J Neuroradiol*. 2023;23:1-9. doi:10.1016/j.neurad.2023.10.009
24. Zhou L, Nguyen TD, Li Y. T2 relaxometry based CSF fraction (CSFF) mapping is a better biomarker for brain drainage pathology than DTI-based free water (DTI-FW) mapping. *Proc Intl Soc Mag Reson Med*. 2022;30:4375.
25. Mosconi L, Rinne JO, Tsui WH, et al. Increased fibrillar amyloid-β burden in normal individuals with a family history of late-onset Alzheimer's. *Proc Natl Acad Sci*. 2010;107(13):5949-5954. doi:10.1073/pnas.0914141107
26. Insel PS, Mormino EC, Aisen PS, Thompson WK, Donohue MC. Neuroanatomical spread of amyloid β and tau in Alzheimer's disease: implications for primary prevention. *Brain Commun*. 2020;2(1):fcaa007. doi:10.1093/braincomms/fcaa007
27. Palmqvist S, Schöll M, Strandberg O, et al. Earliest accumulation of β-amyloid occurs within the default-mode network and concurrently affects brain connectivity. *Nat Commun*. 2017;8:1214. doi:10.1038/s41467-017-01150-x
28. Morris JC. The Clinical Dementia Rating (CDR): current version and scoring rules. *Neurology*. 1993;43(11):2412-a. doi:10.1212/WNL.43.11.2412-a
29. Nasreddine ZS, Phillips NA, Bédirian V, et al. The Montreal cognitive assessment, MoCA: a brief screening tool for mild cognitive impairment. *J Am Geriatr Soc*. 2005;53(4):695-699. doi:10.1111/j.1532-5415.2005.53221.x
30. Besser L, Kukull W, Knopman DS, et al. Version 3 of the National Alzheimer's Coordinating Center's uniform data set.

Alzheimer Dis Assoc Disord. 2018;32(4):351-358. doi:10.1097/WAD.0000000000000279
31. Butler T, Zhou L, Ozsahin I, et al. Glymphatic clearance estimated using diffusion tensor imaging along perivascular spaces is reduced after traumatic brain injury and correlates with plasma neurofilament light, a biomarker of injury severity. *Brain Commun*. 2023;5(3):fcad134. doi:10.1093/braincomms/fcad134
32. Fischl B. FreeSurfer. *NeuroImage*. 2012;62(2):774-781. doi:10.1016/j.neuroimage.2012.01.021
33. Jenkinson M, Beckmann CF, Behrens TEJ, Woolrich MW, Smith SM. FSL. *NeuroImage*. 2012;62(2):782-790. doi:10.1016/j.neuroimage.2011.09.015
34. Villemagne VL, Burnham S, Bourgeat P, et al. Amyloid β deposition, neurodegeneration, and cognitive decline in sporadic Alzheimer's disease: a prospective cohort study. *Lancet Neurol*. 2013;12(4):357-367. doi:10.1016/S1474-4422(13)70044-9
35. Li Y, Tsui W, Rusinek H, et al. Cortical lamina binding of PET amyloid and tau tracers in Alzheimer's disease. *J Nucl Med Off Publ Soc Nucl Med*. 2015;56(2):270-273. doi:10.2967/jnumed.114.149229
36. Rudie JD, Rauschecker AM, Nabavizadeh SA, Mohan S. Neuroimaging of dilated perivascular spaces: from benign and pathologic causes to mimics. *J Neuroimaging Off J Am Soc Neuroimaging*. 2018;28(2):139-149. doi:10.1111/jon.12493
37. Wardlaw JM, Benveniste H, Nedergaard M, et al. Perivascular spaces in the brain: anatomy, physiology and pathology. *Nat Rev Neurol*. 2020;16(3):137-153. doi:10.1038/s41582-020-0312-z
38. Jessen NA, Munk ASF, Lundgaard I, Nedergaard M. The glymphatic system – a beginner's guide. *Neurochem Res*. 2015;40(12):2583-2599. doi:10.1007/s11064-015-1581-6
39. Martinez-Ramirez S, van Rooden S, Charidimou A, et al. Perivascular spaces volume in sporadic and hereditary (Dutch-type) cerebral amyloid angiopathy. *Stroke*. 2018;49(8):1913-1919. doi:10.1161/STROKEAHA.118.021137
40. Mestre H, Verma N, Greene TD, et al. Periarteriolar spaces modulate cerebrospinal fluid transport into brain and demonstrate altered morphology in aging and Alzheimer's disease. *Nat Commun*. 2022;13(1):3897. doi:10.1038/s41467-022-31257-9
41. Kang KM, Byun MS, Yi D, et al. Enlarged perivascular spaces are associated with decreased brain tau deposition. *CNS Neurosci Ther*. 2023;29(2):577-586. doi:10.1111/cns.14040
42. Ding J, Sigurðsson S, Jónsson PV, et al. Large perivascular spaces visible on magnetic resonance imaging, cerebral small vessel disease progression, and risk of dementia: the age, gene/environment susceptibility–Reykjavik study. *JAMA Neurol*. 2017;74(9):1105-1112. doi:10.1001/jamaneurol.2017.1397
43. Lan H, Lynch KM, Custer R, et al. Weakly supervised perivascular spaces segmentation with salient guidance of Frangi filter. *Magn Reson Med*. 2023;89(6):2419-2431. doi:10.1002/mrm.29593
44. Ballerini L, Lovreglio R, Valdés Hernández MdelC, et al. Perivascular spaces segmentation in brain MRI using optimal 3D filtering. *Sci Rep*. 2018;8(1):2132. doi:10.1038/s41598-018-19781-5
45. Pollock H, Hutchings M, Weller RO, Zhang ET. Perivascular spaces in the basal ganglia of the human brain: their relationship to lacunes. *J Anat*. 1997;191(3):337-346. doi:10.1046/j.1469-7580.1997.19130337.x
46. Ineichen BV, Cananau C, Plattén M, et al. Dilated Virchow-Robin spaces are a marker for arterial disease in multiple sclerosis. *eBioMedicine*. 2023;92:104631. doi:10.1016/j.ebiom.2023.104631
47. Du YP, Chu R, Hwang D, et al. Fast multislice mapping of the myelin water fraction using multicompartment analysis of T decay at 3T: a preliminary postmortem study. *Magn Reson Med*. 2007;58(5):865-870. doi:10.1002/mrm.21409
48. Whittall KP, MacKay AL. Quantitative interpretation of NMR relaxation data. *J Magn Reson 1969*. 1989;84(1):134-152. doi:10.1016/0022-2364(89)90011-5
49. Lau LW, Cua R, Keough MB, Haylock-Jacobs S, Yong VW. Pathophysiology of the brain extracellular matrix: a new target for remyelination. *Nat Rev Neurosci*. 2013;14(10):722-729. doi:10.1038/nrn3550
50. MacKay AL, Laule C. Magnetic resonance of myelin water: an in vivo marker for myelin. *Brain Plast*. 2016;2(1):71-91. doi:10.3233/BPL-160033
51. Pasternak O, Sochen N, Gur Y, Intrator N, Assaf Y. Free water elimination and mapping from diffusion MRI. *Magn Reson Med*. 2009;62(3):717-730. doi:10.1002/mrm.22055
52. Bergamino M, Pasternak O, Farmer M, Shenton ME, Paul Hamilton J. Applying a free-water correction to diffusion imaging data uncovers stress-related neural pathology in depression. *NeuroImage Clin*. 2016;10:336-342. doi:10.1016/j.nicl.2015.11.020
53. Yu X, Yin X, Hong H, et al. Increased extracellular fluid is associated with white matter fiber degeneration in CADASIL: in vivo evidence from diffusion magnetic resonance imaging. *Fluids Barriers CNS*. 2021;18(1):29. doi:10.1186/s12987-021-00264-1
54. Raicevic N, Forer JM, Ladrón-de-Guevara A, et al. Sizes and shapes of perivascular spaces surrounding murine pial arteries. *Fluids Barriers CNS*. 2023;20(1):56. doi:10.1186/s12987-023-00454-z
55. Salzman KL, Osborn AG, House P, et al. Giant tumefactive perivascular spaces. *Am J Neuroradiol*. 2005;26(2):298-305.
56. Taoka T, Masutani Y, Kawai H, et al. Evaluation of glymphatic system activity with the diffusion MR technique: diffusion tensor image analysis along the perivascular space (DTI-ALPS) in Alzheimer's disease cases. *Jpn J Radiol*. 2017;35(4):172-178. doi:10.1007/s11604-017-0617-z
57. Hsu JL, Wei YC, Toh CH, et al. Magnetic resonance images implicate that glymphatic alterations mediate cognitive dysfunction in Alzheimer disease. *Ann Neurol*. 2023;93(1):164-174. doi:10.1002/ana.26516

SUPPORTING INFORMATION

Additional supporting information can be found online in the Supporting Information section at the end of this article.

How to cite this article: Zhou L, Nguyen TD, Chiang GC, et al. Parenchymal CSF fraction is a measure of brain glymphatic clearance and positively associated with amyloid beta deposition on PET. *Alzheimer's Dement*. 2024;1-11. https://doi.org/10.1002/alz.13659